Design of SMB for a Nonlinear Amino Acid System with Mass-Transfer Effects

Yi Xie, Chad A. Farrenburg, Chim Y. Chin, Sungyong Mun, and Nien-Hwa L. Wang
School of Chemical Engineering, Purdue University, West Lafayette, IN 47907

A standing wave design (SWD) method and an experimental shortcut design method are developed in this study for SMB systems with nonlinear isotherms and mass-transfer effects (nonideal systems). In the SWD, the mass-transfer correction terms derived in a previous study for linear, nonideal systems are incorporated into the design equations for nonlinear, nonideal systems. The SWD requires accurate isotherm and mass-transfer parameters to ensure high product purity and high yield. If these parameters are unknown, the experimental shortcut design can be applied. Frontal experiments with a binary mixture at a fixed feed concentration and three or more different flow rates are needed to formulate a series of empirical correlations for the SMB design. The two methods were tested for the binary separation of phenylalanine and tryptophan. Both rated model simulations and experimental data showed that high product purity (99.1%–100%) and high yield (96.3%–100%) were achieved in both methods. The experimental shortcut design method is simpler than the SWD, but is limited to a fixed feed concentration. A dimensionless number is derived to quantify the deviation of an actual nonideal system from a system without mass-transfer effects (ideal system). If the dimensionless number has a value greater than 0.005 for the binary amino acid separation, the system deviates from its corresponding ideal system and the design considering mass-transfer effects gives significantly higher purity and yield than the ideal design.

Introduction

When chromatography is employed at a preparative or process scale, it is often advantageous in terms of solvent consumption and sorbent productivity to use simulated moving bed (SMB) technology (Schulte et al., 1996). SMB was originally developed at UOP for petrochemical separations (Broughton and Gerhold, 1961). A standard four-zone SMB unit for binary separations consists of a continuous ring of columns divided by four ports. Two of these ports are inlets: one for a feed solution and the other for an eluent (or desorbent). The other two are outlets: one for the compound with a higher affinity to the stationary phase (the extract) and the other for the compound with a lower affinity (the raffinate). These inlet and outlet ports move periodically in the direction of the fluid flow, such that the feed is continuously loaded into the overlapping region of the two components, while the extract and the raffinate are drawn from the separated regions.

A large number of SMB processes have been developed for the separation of petrochemicals and the preparation of high-fructose corn syrup (Ruthven and Ching, 1989; Ganetsos and Barker, 1993). Since the early 1990s, SMB processes have been used extensively for chiral separations (Juza et al., 2000; Schulte and Strube, 2001). One of the largest SMB (with 800 mm I.D. columns) for chiral separations has been installed at Aerojet Fine Chemicals (Sacramento, CA) by Novasep (Vandoeuvre-lès-Nancy, France). SMB has also been applied for other bioseparations, such as protein or amino acid desalting, protein purification, and antibody purification (Nicoud, 1998; Imamoglu, 2002). Two examples of amino acid separations were presented in the review article by Imamoglu

Correspondence concerning this article should be addressed to N.-H. L. Wang.

(2002). One example was regarding the large-scale production of lysine and the other was related to the separation of L-glutathione and glutamic acid. Another example of amino acid separation was reported by Wu et al. (1998) and Xie et al. (2000). In their studies, phenylalanine and tryptophan were separated using a ten-column SMB packed with a PVP resin.

Chromatography or SMB columns are often overloaded to gain higher productivity, in particular when expensive adsorbents such as chiral stationary phases are used. Overloading often results in nonlinear adsorption behavior. This study focuses on the design of SMB with nonlinear isotherms. One of the key issues in SMB design is the determination of zone flow rates and switching time.

The triangle theory, which is derived from equilibrium theory (Rhee et al., 1971), has been widely used in the design of SMB processes (Storti et al., 1989, 1993; Mazzotti et al., 1997). The triangle theory specifies a triangular region, which encloses all feasible operating conditions that guarantee 100% purity and yield for an ideal system, in which mass-transfer effects are negligible. The triangular region is identified in a plot of two flow rate ratios m_2 and m_3, which are the net flow ratios of fluid phase to solid phase in the two zones upstream and downstream, respectively, from the feed port.

An ideal system, however, normally requires fine adsorbent particles, high pressure, and high equipment cost. A low-pressure system with large adsorbent particles is often more economical (Pynnonen, 1998). The mass-transfer effects in low-pressure systems are significant. A system with significant mass-transfer effects is defined as a nonideal system to distinguish it from the ideal system.

The mass-transfer effects on SMB performance have been investigated by many researchers. Zhong and Guiochon (1997) and Yun et al. (1997) used an equilibrium-dispersive model to study the mass-transfer effects on linear isotherm systems. Their simulations showed that the product purities could be lower than 90% for a system with a selectivity of 1.1 and 1,000 theoretical plates. Pais et al. (1997) modeled a process for the separation of 1,1′-bi-2-naphthol enantiomers, which exhibit nonlinear adsorption behavior. Significant band broadening was shown to occur with increasing mass-transfer resistance. Azevedo and Rodrigues (1999), Migliorini et al. (1999), and Biressi et al. (2000) found that the triangular region for a nonideal system was substantially smaller than the triangular region for a corresponding ideal system.

In order to determine the operating conditions for nonideal systems, Biressi et al. (2000) proposed an algorithm based on the triangle theory and numerical simulations. A large number of computer simulations are used to find the triangular region that guarantees the desired purity and yield for a given set of mass-transfer parameters. A safety margin method was developed based on the equilibrium theory, but provided an empirical margin to counter the mass-transfer effects (Ching et al., 1985; Ruthven and Ching, 1989; Zhong and Guiochon, 1997). Azevedo and Rodrigues (1999) extended the previous two methods to a separation volume analysis, in which operating conditions were confined within a series of distorted triangular region in a 3-D domain. The separation volume analysis was implemented for fructose-glucose separation within a linear isotherm range (Azevedo and Rodrigues, 2001).

Ma and Wang (1997) developed a standing wave design (SWD) method, which provided an exact margin to counter the mass-transfer effects in linear isotherm systems. This method does not require any trial-and-error. Both theoretical and experimental studies have shown that the SWD is efficient and guarantees high purity and high yield for binary separations (Wu et al., 1998; Xie et al., 2000) and multicomponent separations (Hritizko et al., 2002; Xie et al., 2002) with linear isotherms.

The SWD was also developed for nonlinear isotherm systems without mass-transfer effects (Mallmann et al., 1998). In this study, the SWD is extended to nonlinear, nonideal systems. The mass-transfer correction terms derived for linear, nonideal systems are used as approximations to counter the mass-transfer effects in nonlinear systems. Separation of a binary amino acid mixture of phenylalanine and tryptophan is used to validate the design method. Both numerical simulations and experimental results show that high purity and high yield are achieved.

If the isotherm parameters are unknown, Mallmann et al. (1998) pointed out that the standing wave velocities could be estimated from a frontal-and-elution experiment with a binary mixture. Migliorini et al. (2002) also developed a shortcut experimental method to obtain an approximate triangular region without measuring the isotherm parameters. Neither of these two shortcut design methods considers the mass-transfer effects. In this study, an efficient shortcut design method for nonlinear, nonideal systems is developed without measurement of the isotherm and mass-transfer parameters. This design method is also validated with the phenylalanine-tryptophan system.

A dimensionless number is derived to estimate the nonideality or the deviation of a nonideal system from its corresponding ideal system. The results show that the dimensionless number is inversely proportional to product purities based on a design without considering mass-transfer effects (ideal design). If the dimensionless number is greater than 0.005, mass-transfer effects must be considered in the SMB design for the two amino acids separation to ensure high purity and high yield.

Theory

Standing wave design for ideal systems

The key idea in the SWD is to set the switching time and the flow rate in each zone, such that the key concentration wave (boundary of a solute band) in each zone migrates at the same speed as the periodic port movement. As a result, all waves remain *standing* with respect to the ports. The standing waves of a binary system are component 2 desorption wave in zone I, component 1 desorption wave in zone II, component 2 adsorption wave in zone III, and component 1 adsorption wave in zone IV (Figure 1). Under the standing wave conditions, the SMB system reaches its maximum throughput and minimum solvent consumption for a given feed flow rate (Ma and Wang, 1997).

In order to achieve the standing wave conditions, Mallmann et al. (1998) derived a set of equations to determine the zone flow rates and switching time for a binary ideal system with nonlinear isotherms (Langmuir and Anti-Langmuir).

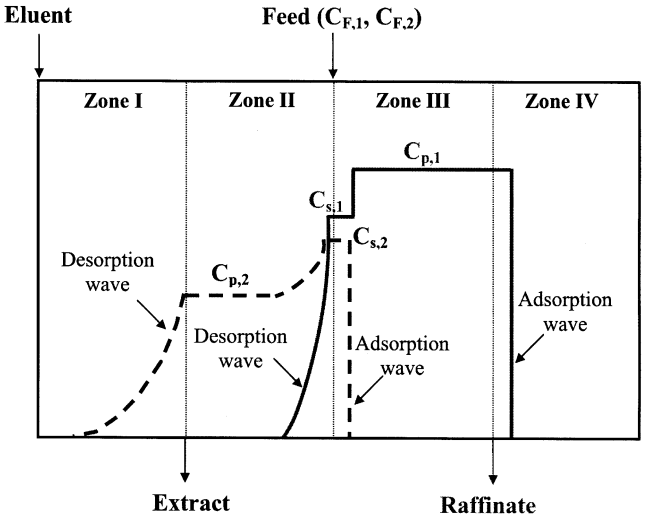

Figure 1. Profiles of a binary system with nonlinear isotherms (Langmuir) without mass-transfer effects.

Solid lines denote the low affinity component (1) and dashed lines denote the high affinity component (2).

These SWD equations are given by

$$\frac{u_0^{\mathrm{I}}}{\left(1+P\delta_2^{\mathrm{I}}\right)}-\nu=0 \tag{1a}$$

$$\frac{u_0^{\mathrm{II}}}{\left(1+P\delta_1^{\mathrm{II}}\right)}-\nu=0 \tag{1b}$$

$$\frac{u_0^{\mathrm{III}}}{\left(1+P\delta_2^{\mathrm{III}}\right)}-\nu=0 \tag{1c}$$

$$\frac{u_0^{\mathrm{IV}}}{\left(1+P\delta_1^{\mathrm{IV}}\right)}-\nu=0 \tag{1d}$$

where the subscripts 1 and 2 denote the low and high affinity solutes, respectively; the superscripts I, II, III, IV denote the four zones; ν is the average port velocity (= column length/switching time); u_0^j is the interstitial velocity in zone j; P is the phase ratio, defined as $(1-\epsilon_b)/\epsilon_b$; ϵ_b is the interparticle voidage; and the effective retention factors (δ) for the Langmuir isotherm binary system are calculated as follows

$$\delta_2^{\mathrm{I}}=\epsilon_p+\left(1-\epsilon_p\right)a_2 \tag{2a}$$

$$\delta_1^{\mathrm{II}}=\epsilon_p+\left(1-\epsilon_p\right)\left(\frac{a_1}{1+b_2C_{p,2}}\right) \tag{2b}$$

$$\delta_2^{\mathrm{III}}=\epsilon_p+\left(1-\epsilon_p\right)\left(\frac{a_2}{1+b_1C_{s,1}+b_2C_{s,2}}\right) \tag{2c}$$

$$\delta_1^{\mathrm{IV}}=\epsilon_p+\left(1-\epsilon_p\right)\left(\frac{a_1}{1+b_1C_{p,1}}\right) \tag{2d}$$

where ϵ_p is the intraparticle voidage; a and b are Langmuir isotherm parameters; and $C_{p,i}$ and $C_{s,i}$ are plateau concentrations of component i, as shown in Figure 1. Note that the δ values in zones II–IV vary with the concentrations of both components. The feed flow rate (F_F) is related to the interstitial velocities of zones II and III as follows

$$\frac{F_F}{\epsilon_b S}=u_0^{\mathrm{III}}-u_0^{\mathrm{II}} \tag{3}$$

where S is the cross-sectional area of the column.

If the plateau concentrations in Eq. 2 are known, Eqs. 1–3 can be directly solved to obtain the zone flow rates and switching time, which satisfy the standing wave conditions for a given feed flow rate and feed concentration. The plateau concentrations, however, are dependent upon the feed concentrations and SMB operating conditions; thus, are unknown *a priori*. Mallmann et al. (1998) developed a procedure to solve the problem. The initial zone flow rates and switching time were calculated from the estimated plateau concentrations. The operating conditions were then used to solve a set of partial differential equations (PDE) for the SMB process. The plateau concentrations obtained from the PDE solutions were then used to solve Eqs. 1–3. This procedure was repeated until the resulting zone flow rates and switching time remained constant.

In this study, a simpler procedure without solving the PDE is developed to solve Eqs. 1–3. Figure 2 shows this procedure. Initially guessed $C_{s,1}$ and $C_{s,2}$ are used to calculate $C_{p,1}$ and $C_{p,2}$, following the procedure of Mallmann et al. (1998). The C_s and C_p values are then substituted into Eqs. 1–3 to calculate the zone flow rates and switching time. Note that the initially guessed $C_{s,1}$ and $C_{s,2}$ should be much lower than the feed concentrations ($C_{F,1}$ and $C_{F,2}$); otherwise, there may be no feasible solutions of Eqs. 1 and 3 if the selectivity is low. Once the zone flow rates and switching time are known, a mass-balance equation between the feed port and the raffinate port is used to estimate a new $C_{p,1}$ value. A new $C_{p,2}$ value is calculated from the feed concentrations using the hodograph solution (Mallmann et al., 1998). If the new $C_{p,1}$ and $C_{p,2}$ values equal the initially calculated values, then the iteration is complete. Otherwise, new $C_{s,1}$ and $C_{s,2}$ values are needed to replace the initial guesses to start next round of calculation. The procedure is repeated until the plateau concentrations remain unchanged.

In order to account for the delay caused by extra column dead volume (DV), an apparent retention factor δ^* is derived as

$$\delta^*=\delta+\frac{DV}{PL_cS\epsilon_b} \tag{4}$$

where L_c is the single column length. The apparent retention factor δ^* can be substituted into Eqs. 1–3 to counter the delay effect caused by the extra-column dead volume.

Standing wave design for nonideal systems

Equation 1 is derived for an ideal system, in which mass-transfer effects are ignored. In a nonideal system, however,

mass-transfer effects cause concentration wave spreading and cannot be ignored in the SMB design. Ma and Wang (1997) derived a set of equations to determine the zone flow rates and switching time for linear, nonideal systems, such that the mass-transfer spreading can be compensated. In these equations, mass-transfer correction terms are added to modify the standing wave equations for linear, ideal systems. These mass-transfer correction terms are similarly applied in this study to account for the mass-transfer effects in a nonlinear, nonideal system as follows

$$\frac{u_0^{\mathrm{I}}}{\left(1+P\delta_2^{\mathrm{I}}\right)}-\nu=\frac{\beta_2^{\mathrm{I}}}{\left(1+P\delta_2^{\mathrm{I}}\right)L^{\mathrm{I}}}\left(E_{b,2}^{\mathrm{I}}+\frac{P\nu^2\left(\delta_2^{\mathrm{I}}\right)^2}{k_2^{\mathrm{I}}}\right) \quad (5a)$$

$$\frac{u_0^{\mathrm{II}}}{\left(1+P\delta_1^{\mathrm{II}}\right)}-\nu=\frac{\beta_1^{\mathrm{II}}}{\left(1+P\delta_1^{\mathrm{II}}\right)L^{\mathrm{II}}}\left(E_{b,1}^{\mathrm{II}}+\frac{P\nu^2\left(\delta_1^{\mathrm{II}}\right)^2}{k_1^{\mathrm{II}}}\right) \quad (5b)$$

$$\frac{u_0^{\mathrm{III}}}{\left(1+P\delta_2^{\mathrm{III}}\right)}-\nu=-\frac{\beta_2^{\mathrm{III}}}{\left(1+P\delta_2^{\mathrm{III}}\right)L^{\mathrm{III}}}\left(E_{b,2}^{\mathrm{III}}+\frac{P\nu^2\left(\delta_2^{\mathrm{III}}\right)^2}{k_2^{\mathrm{III}}}\right) \quad (5c)$$

$$\frac{u_0^{\mathrm{IV}}}{\left(1+P\delta_1^{\mathrm{IV}}\right)}-\nu=-\frac{\beta_1^{\mathrm{IV}}}{\left(1+P\delta_1^{\mathrm{IV}}\right)L^{\mathrm{IV}}}\left(E_{b,1}^{\mathrm{IV}}+\frac{P\nu^2\left(\delta_1^{\mathrm{IV}}\right)^2}{k_1^{\mathrm{IV}}}\right) \quad (5d)$$

where L^j is the length of zone j; $E_{b,i}^j$ is the axial dispersion coefficient of component i in zone j; and k_i^j is the lumped mass-transfer parameter of component i in zone j and is defined as

$$\frac{1}{k_i^j}=\frac{R_p^2}{15\epsilon_p D_{p,i}}+\frac{R_p}{3k_{f,i}^j} \qquad (i=1,2) \quad (6)$$

where R_p is the particle radius; $D_{p,i}$ is the intraparticle diffusivity of component i; and $k_{f,i}^j$ is the film mass-transfer coefficient of component i in zone j. β is the logarithm of the ratio of the highest concentration to the lowest concentration of a standing wave in a particular zone. β is an index of product purity and yield; the larger the β value, the higher the product purity and yield (Ma and Wang, 1997; Xie et al., 2000; Hritzko et al., 2002).

Compared with Eqs. 1a–1d, Eqs. 5a–5d have additional terms on the righthand sides. These additional terms modify the zone flow rates and switching time, such that the desorption waves in zones I and II move faster than the port movement, whereas the adsorption waves in zones III and IV move slower than the port movement. As a result, the wave spreading caused by mass-transfer effects is overcome and the wave centers are *pinched* at the boundaries. Note that the righthand sides are the same as those derived by Ma and Wang (1997) for linear systems. For zones I and II, the nonlinear desorption wave spreading due to mass-transfer effects is similar to that in linear systems. The linear mass-transfer corrections are appropriate in zones I and II for nonlinear systems. However, the adsorption waves in zones III and IV are self-sharpening in nonlinear (Langmuir) systems; thus, the linear mass-transfer corrections in zones III and IV are overestimated for nonlinear systems. Therefore, the design given by Eqs. 5a–5d is conservative.

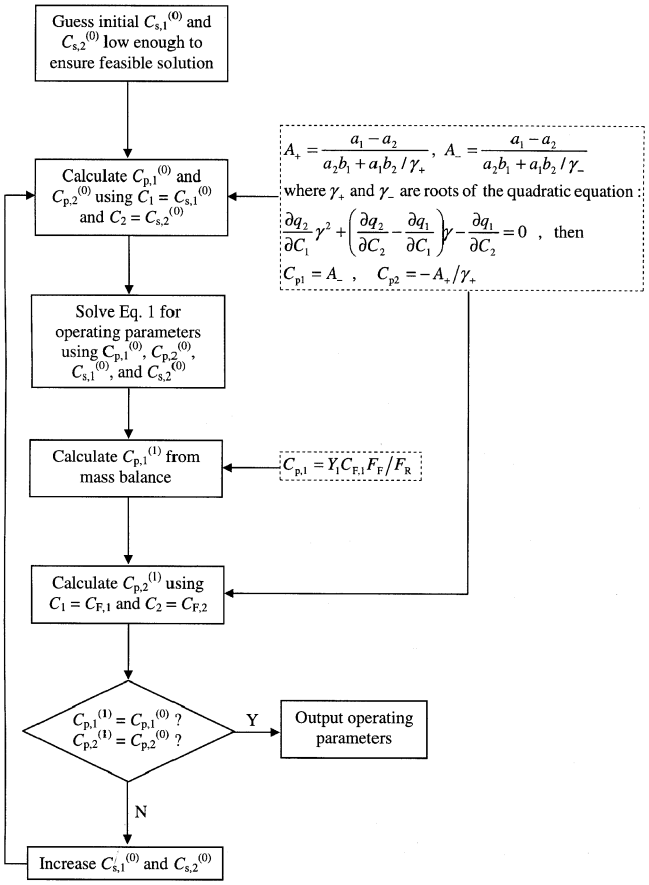

Figure 2. Iteration procedure for calculating the plateau concentrations in Eq. 1.

The same procedure used to solve Eqs. 1–3 can be applied to solve Eqs. 2, 3, and 5. If there is no pressure drop limit, Eqs. 1–3 can be solved for any feed flow rate. There is no maximum feed flow rate for an ideal system. However, a maximum feed flow rate exists for a nonideal system even without a pressure drop limit. The maximum feed flow rate can be derived from Eqs. 2, 3, and 5. Combining Eqs. 3, 5b, and 5c, one can obtain the following equation

$$\left[\frac{P\beta_2^{\mathrm{III}}\left(\delta_2^{\mathrm{III}}\right)^2}{k_2^{\mathrm{III}}L^{\mathrm{III}}}+\frac{P\beta_1^{\mathrm{II}}\left(\delta_1^{\mathrm{II}}\right)^2}{k_1^{\mathrm{II}}L^{\mathrm{II}}}\right]\nu^2-P\left(\delta_2^{\mathrm{III}}-\delta_1^{\mathrm{II}}\right)\nu+\frac{F_F}{\epsilon_b S}+\frac{\beta_2^{\mathrm{III}}E_{b,2}^{\mathrm{III}}}{L^{\mathrm{III}}}+\frac{\beta_1^{\mathrm{II}}E_{b,1}^{\mathrm{II}}}{L^{\mathrm{II}}}=0 \quad (7)$$

Equation 7 has solutions only if the following equality is satisfied

$$P^2\left(\delta_2^{\mathrm{III}}-\delta_1^{\mathrm{II}}\right)^2-4\left[\frac{P\beta_2^{\mathrm{III}}\left(\delta_2^{\mathrm{III}}\right)^2}{k_2^{\mathrm{III}}L^{\mathrm{III}}}+\frac{P\beta_1^{\mathrm{II}}\left(\delta_1^{\mathrm{II}}\right)^2}{k_1^{\mathrm{II}}L^{\mathrm{II}}}\right]\times\left(\frac{F_F}{\epsilon_b S}+\frac{\beta_2^{\mathrm{III}}E_{b,2}^{\mathrm{III}}}{L^{\mathrm{III}}}+\frac{\beta_1^{\mathrm{II}}E_{b,1}^{\mathrm{II}}}{L^{\mathrm{II}}}\right)\geq 0 \quad (8)$$

The maximum feed flow rate (F_F) for a given SMB system can be calculated from Eq. 8. Since δ_i^j, $E_{b,i}^j$, and k_i^j are dependent on the operating conditions, the maximum F_F needs to be solved simultaneously with Eqs. 5a–5d.

Dimensionless number to characterize nonideality

As shown above, the SWD for ideal systems (ideal design) is much simpler than the SWD for nonideal systems (nonideal design). If a system has negligible mass-transfer resistance and is close to an ideal system, the ideal design is preferred; otherwise, the nonideal design is required. Currently, there is no simple and efficient way to tell how close a system is to the corresponding ideal system and under what conditions the nonideal design should be used. A dimensionless number is proposed to characterize the deviation of a nonideal system from the corresponding ideal system. The SWD equations for nonideal systems (Eq. 5) can be rearranged as follows

$$1-\frac{\left(1+P\delta_2^{\mathrm{I}}\right)\nu}{u_0^{\mathrm{I}}}=\beta_2^{\mathrm{I}}DI_2^{\mathrm{I}} \tag{9a}$$

$$1-\frac{\left(1+P\delta_1^{\mathrm{II}}\right)\nu}{u_0^{\mathrm{II}}}=\beta_1^{\mathrm{II}}DI_1^{\mathrm{II}} \tag{9b}$$

$$1-\frac{\left(1+P\delta_2^{\mathrm{III}}\right)\nu}{u_0^{\mathrm{III}}}=-\beta_2^{\mathrm{III}}DI_2^{\mathrm{III}} \tag{9c}$$

$$1-\frac{\left(1+P\delta_1^{\mathrm{IV}}\right)\nu}{u_0^{\mathrm{IV}}}=-\beta_1^{\mathrm{IV}}DI_1^{\mathrm{IV}} \tag{9d}$$

where the dimensionless number DI (deviation from ideality) is defined as

$$DI_i^j\equiv\frac{1}{Pe_i^j}+\frac{1}{St_i^j}P\left(\delta_i^j\right)^2\left(\frac{\nu}{u_0^j}\right)^2\left(\frac{R_p}{L^j}\right) \tag{10}$$

and the Peclet number (Pe_i^j) and the Stanton number (St_i^j) for component i in zone j are defined as

$$Pe_i^j=\frac{u_0^jL^j}{E_{b,i}^j} \tag{11a}$$

$$St_i^j=\frac{k_i^jR_p}{u_0^j}=\frac{1}{u_0^j\left(\dfrac{R_p}{15\epsilon_pD_{p,i}}+\dfrac{1}{3k_{f,i}^j}\right)} \tag{11b}$$

DI is an index that can be used to measure how much a system deviates from its corresponding ideal system. The larger DI is, the more the system deviates from the ideal system. As DI approaches zero, the system becomes ideal. Since zones II and III are the key separation zones, in which the operating conditions significantly affect the product purities, only the dimensionless numbers of zones II and III (DI_1^{II} and DI_2^{III}) are needed. A detailed discussion on DI for the binary amino acid system is given in the results and discussion section.

Experimental shortcut design

Mallmann et al. (1998) and Migliorini et al. (2002) proposed similar shortcut experimental methods for SMB design, which did not require the isotherm parameters. In both studies, frontal experiments and hodograph analysis were used, and mass-transfer effects were neglected.

In this study, an experimental design procedure is proposed to include the mass-transfer effects in the design. The following equations are needed to derive the design equations for an SMB process: (1) correlation between the shockwave velocity and the flow rate; (2) correlation between the mass-transfer zone length and the flow rate; and (3) correlation between the diffuse wave velocity and the flow rate. These empirical correlations, which can be estimated from the long pulse (including frontal and elution) tests of a binary mixture, are given with unknown coefficients as follows

$$u_{sh,1}=x_1F \tag{12a}$$

$$u_{sh,2}=x_2F \tag{12b}$$

$$L_{\mathrm{MTZ},1}=x_3F+y_3 \tag{13a}$$

$$L_{\mathrm{MTZ},2}=x_4F+y_4 \tag{13b}$$

$$u_{\mathrm{diff},1}=x_5F+y_5 \tag{14a}$$

$$u_{\mathrm{diff},2}=x_6F+y_6 \tag{14b}$$

where u is the wave velocity (m/s) and x and y are coefficients estimated from long pulse tests; subscripts sh, diff, and MTZ denote shockwave, diffuse wave, and mass-transfer zone, respectively.

Equation 12 can be derived from the local equilibrium theory (Rhee et al., 1971) for a given feed concentration and a fixed column dimension. Equation 13 describes a linear relation between the mass-transfer zone length (L_{MTZ}) and the flow rate. A similar equation was described by Hritzko et al. (2000). In their study, if the flow rate was zero, the associated L_{MTZ} was zero. However, if the column is not sufficiently long and the constant pattern of the shockwave is not fully developed, the experimentally measured L_{MTZ} could be shorter at high flow rates. Thus, the interception terms in Eq. 13 may be nonzero as shown later in the results and discussion section. Equation 14 correlates the diffuse wave velocity with the flow rate. Note that the experimentally measured diffuse wave velocity depends on both the thermodynamics and kinetics of the system. The linear correlation in Eq. 14 is an approximation, and its validity is explained later in the results and discussion section.

On the basis of the above correlations, the SMB design procedure is as follows:

(1) The concentration waves migrate by one column length between two consecutive switchings in SMB. To maintain the shockwave of component 2 in zone III, L^{III} is set equal to $L_{\mathrm{MTZ},2}+L_c$. As an SMB approaches a true moving bed, L_c approaches zero and L^{III} equals $L_{\mathrm{MTZ},2}$. The flow rate of zone III (F^{III}) can be estimated from Eq. 13b with the $L_{\mathrm{MTZ},2}$.

(2) Calculate the shockwave velocity (u_{sh}) of component 2 from Eq. 12b by setting F equal to F^{III}.

(3) In order to let the adsorption wave of component 2 stand in zone III, the average port velocity (ν) is set equal to u_{sh} of component 2.

(4) Similarly, ν is set equal to u_{sh} of component 1 and the zone IV flow rate (F^{IV}) is estimated from Eq. 12a.

(5) For a given feed flow rate (F_F), the flow rate of zone II (F^{II}) is given by the difference between F^{III} and F_F.

(6) The zone I flow rate (F^{I}) is estimated from Eq. 14b by setting the diffuse wave velocity (u_{diff}) of component 2 equal to ν, such that the diffuse wave of component 2 stands in zone I.

The following design equations are derived based on the above procedure

$$F^{\mathrm{I}} = \frac{(\nu - y_6)}{x_6} \tag{15a}$$

$$F^{\mathrm{II}} = F^{\mathrm{III}} - F_F \tag{15b}$$

$$F^{\mathrm{III}} = \frac{\left(L^{\mathrm{III}} - L_c\right) - y_4}{x_4} \tag{15c}$$

$$F^{\mathrm{IV}} = \frac{\nu}{x_1} \tag{15d}$$

$$\nu = u_{sh} = x_2 F^{\mathrm{III}} \tag{15e}$$

In Eqs. 15a–15e, F^{I}, F^{II}, F^{III}, F^{IV}, and ν are the only unknowns for a given SMB equipment and feed flow rate at a fixed feed concentration.

According to the preceding design step 5, the zone II flow rate (F^{II}) is determined by the difference between the zone III flow rate (F^{III}) and the given feed flow rate (F_F). The estimated F^{II}, however, cannot guarantee that the desorption wave of component 1 will stand in zone II. In order to prevent component 1 from contaminating the extract, the desorption or diffuse wave velocity of component 1 ($u_{\mathrm{diff},1}$), which can be calculated from Eq. 14a with the estimated F^{II}, should be greater than or equal to the average port velocity (ν). This is given by

$$F^{\mathrm{II}} \geq \frac{\nu - y_5}{x_5} \tag{16}$$

If Eq. 16 cannot be satisfied with the estimated F^{II}, the feed flow rate should be reduced or the length of zone III should be increased. Equation 16 can thus be used in combination with Eqs. 15b and 15c to estimate the maximum feed flow rate for a given SMB equipment. Note that pressure drop limitation is not considered here.

The estimation of the zone IV flow rate (F^{IV}) from the design step 4 is based on the standing condition of the component 1 shockwave ($u_{sh,1}$ equals ν). To prevent component 1 from entering zone I and cross-contaminating the extract, the spreading of the adsorption wave should be confined within zone IV. For this reason, the mass-transfer zone length of component 1 ($L_{\mathrm{MTZ},1}$), which is calculated from Eq. 13a with the estimated F^{IV}, should be less than or equal to $L^{\mathrm{IV}} - L_c$

$$F^{\mathrm{IV}} \leq \frac{\left(L^{\mathrm{IV}} - L_c\right) - y_3}{x_3} \tag{17}$$

If Eq. 17 cannot be satisfied with the estimated F^{IV}, the length of zone IV should be increased.

Experimental

Materials

HPLC grade acetonitrile and methanol were purchased from Fisher Scientific (Fairlawn, NJ). Distilled deionized water (DDW) was obtained through a Milli-Q system by Millipore (Milford, MA). Two amino acids, L-phenylalanine (phe, MW 165) and L-tryptophan (trp, MW 204) with 98% minimum purities (TLC), were purchased from Sigma Chemical Co. (Milwaukee, WI).

PVP resin (poly-4-vinylpyridine cross-linked, Reillex HP polymer) from Reilly Industries Inc. (Indianapolis, IN) was used as the sorbent for amino acid separation. This resin is stable, easily regenerable, and commercially available.

The glass columns for packing the PVP resins were purchased from Ace Glass Inc. (Louisville, KY). Each column is 30.5 cm in length and 2.68 cm in inner diameter. A YMC ODS-AQ HPLC column (5 μm, 120 Å, 4.6×250 mm) was purchased from Waters Corporation (Milford, MA) for the assay of the amino acids phe and trp.

Equipment

A Pharmacia (Piscataway, NJ) fast protein liquid chromatography (FPLC) system was used in the batch chromatography experiments. This system consisted of two pumps (Pharmacia P-500), a liquid chromatography controller (Pharmacia LCC-500), an injection valve (Pharmacia MV-7), and a fraction collector (Pharmacia Frac-100). Data monitoring and collection were handled with a photodiode array detector (Waters 990) and accompanying data collection software.

The HPLC system for phe-trp sample assay consisted of two pumps (Waters 510), a tunable single-wavelength detector (Waters 486), and an injector (Rheodyne Model 7010). Waters Millennium 2010 software operated in a Windows environment was used for data collection and analysis.

Two SMB units were used in this study. One unit (SMB1) was purchased from Advanced Separation Technologies Incorporation (Lakeland, FL). SMB1 consisted of a controller for the adjustment of the switching time and a frame that supports a rotation gear, a drive assembly, and a column rack. Ten columns were used in SMB1 and the zone configuration (allocation of the 10 columns in the four zones) was 3-2-3-2. A second unit (SMB2) was built in-house. The details of this unit have been described by Chin (2001). Eight columns were used in SMB2 and the zone configuration was 2-2-2-2.

Four single-piston positive displacement pumps were purchased from Fluid Metering Inc. (Syosset, NY). Each pump consists of a pump head with adjustable stroke length (Model RHV) and a stroke rate controller (Model V200). The flow rate can be adjusted instantaneously by changing the stroke

length or the stroke rate. Two pumps controlled the inlet flow rates, one for the feed and the other for the eluent. Another two pumps controlled the zone II and zone IV flow rates, respectively. The extract flow rate was determined by the difference between the zone I flow rate and zone II flow rate. The raffinate flow rate was determined by the difference between the zone III flow rate and zone IV flow rate. A differential pressure flow meter was purchased from Cole-Parmer Instrument Company (Vernon Hills, IL) and installed at the outlet of the zone IV pump to monitor the zone IV flow rate. Two digital balances (Champ Bench Scale) were purchased from Ohaus Corporation (Florham Park, NJ) and used to monitor the amount of the feed and the eluent. The average flow rates of feed and eluent were estimated from the weight changes within a switching period.

Procedure

HPLC Assay. The YMC ODS-AQ HPLC column was used in the assay to determine the concentration of the mixtures of phe and trp. The mobile phase consisted of DDW and acetonitrile in a ratio of 4:1 (v/v), and was sonicated and degassed for half an hour prior to use. The flow rate was 8.33×10^{-9} m^3/s and the injection volume was 5×10^{-9} m^3. The chromatograms were examined at a wavelength of 260 nm. The sample analysis time was 900 s. Each sample was assayed twice to ensure accuracy.

Estimation of the Bed Voidage. Methanol is an effective regenerant for removing weakly adsorbed species from the PVP resin. Phenylalanine has no affinity to the resin in pure methanol, and it can be used as an inert tracer to measure the total voidage. A 2.0×10^{-6} m^3 of phe pulse was injected into the column pre-equilibrated with pure methanol. The mobile phase flow rate was 3.33×10^{-8} m^3/s. The total voidage of the column (ϵ_t) can be estimated from the first moment of the phe pulse chromatogram. Since the particle porosity (ϵ_p) was provided by the resin manufacturer, the bed voidage (ϵ_b) can be calculated from the following equation

$$\epsilon_b = \frac{\epsilon_t - \epsilon_p}{1 - \epsilon_p} \tag{18}$$

Long Pulses of the Mixture of Phe and Trp. The long pulse experiment included a frontal containing a mixture of phe (5.5 kg/m^3) and trp (2.0 kg/m^3), followed by elution with DDW. The effluent stream was monitored with a UV detector at 260 nm and continuously collected with a fraction collector. The collected sample size was 5×10^{-6} m^3. The samples were assayed with the HPLC. Three long pulse experiments at different flow rates (8.33×10^{-8} m^3/s, 1.25×10^{-7} m^3/s, 1.67×10^{-7} m^3/s) were conducted.

Results and Discussion

Long pulses of the Phe-Trp mixture

The long pulse chromatograms are shown in Figure 3. The symbols are experimental data and the lines are the simulation results. A detailed rate model, which has been described in previous studies (Hritzko et al., 2002; Xie et al., 2002), is used for the simulations. The isotherm and mass-transfer parameters of phe and trp used in the simulations have been reported in a previous study (Wu et al., 1998). These parameters are listed in Table 1. Note that the simulations are used only to validate the shortcut design method in this study. The design itself is independent of the simulation results. However, the experimental data can be used to benchmark the model parameters using these simulations.

From the chromatograms of the long pulse experiments, one can obtain several empirical correlations (Eqs. 12–14), which are needed in the shortcut design of SMB. The shockwave velocities are calculated by dividing the column length by the mass center times of the adsorption waves (or frontal waves). The mass-transfer zone length for each component equals the product of the shockwave velocity and the time span associated with the 5–95% plateau concentration portion of the adsorption wave. The diffuse wave velocities are estimated from the column length and the 5% plateau concentration points on the diffuse waves. Note that the time used in the diffuse wave velocity calculations starts from the moment when the washing step begins. The mass-transfer zone length (L_{MTZ}), shockwave velocity, and the diffuse wave

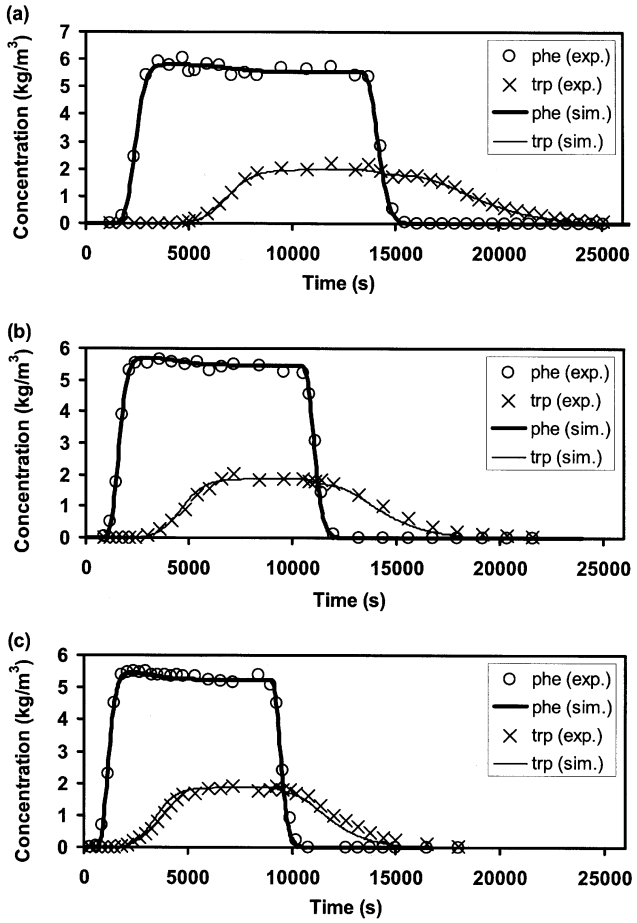

Figure 3. Long pulse experimental data and simulation results at the flow rate of (a) 8.33×10^{-8} m^3/s, (b) 1.25×10^{-7} m^3/s, and (c) 1.67×10^{-7} m^3/s.

exp.—experiment, sim.—simulation.

Table 1. Isotherm Parameters (298 K), Mass-Transfer Parameters, and Numerical Simulation Parameters

	Isotherm Parameters	
	a^*	b
Phe	1.61	0.0153
Trp	12.3	0.161
	Mass-Transfer Parameters	
E_b (m^2/s)	The Chung and Wen correlation	
k_f (m/s)	The Wilson and Geankoplis correlation	
D_∞ (m^2/s)	6.80×10^{-10}	
D_p (m^2/s)	1.09×10^{-10}	
	Numerical Parameters	
Axial elements	Collocation points: Axial / Particle	Absolute tolerance / Relative tolerance
80	4 / 2	0.0001 / 0.001

* The Langmuir isotherm parameter a is based on solid volume.

velocity are plotted against the flow rate in Figure 4. The coefficients x and y in Eqs. 12–14 are regressed from the data shown in Figure 4 and listed in Table 2.

The coefficients y_5 and y_6 are non-zero (Table 2), which indicates that the diffuse wave velocity is not zero as the flow rate approaches zero (Eqs. 14a and 14b). To understand this result, the simulated elution curves of trp with and without mass-transfer effects are plotted in Figure 5. The column is saturated with trp before elution. The elution curve of trp

Table 2. Coefficients of the Correlations from the Long Pulse Experiments

x_1 (m^{-2})	x_2 (m^{-2})	x_3 (s/m^2)	x_4 (s/m^2)	x_5 (m^{-2})	x_6 (m^{-2})
1.53×10^3	5.29×10^2	7.35×10^5	1.02×10^6	1.52×10^3	3.23×10^2
		y_3 (m)	y_4 (m)	y_5 (m/s)	y_6 (m/s)
		1.02×10^{-1}	7.03×10^{-2}	1.45×10^{-5}	2.53×10^{-6}

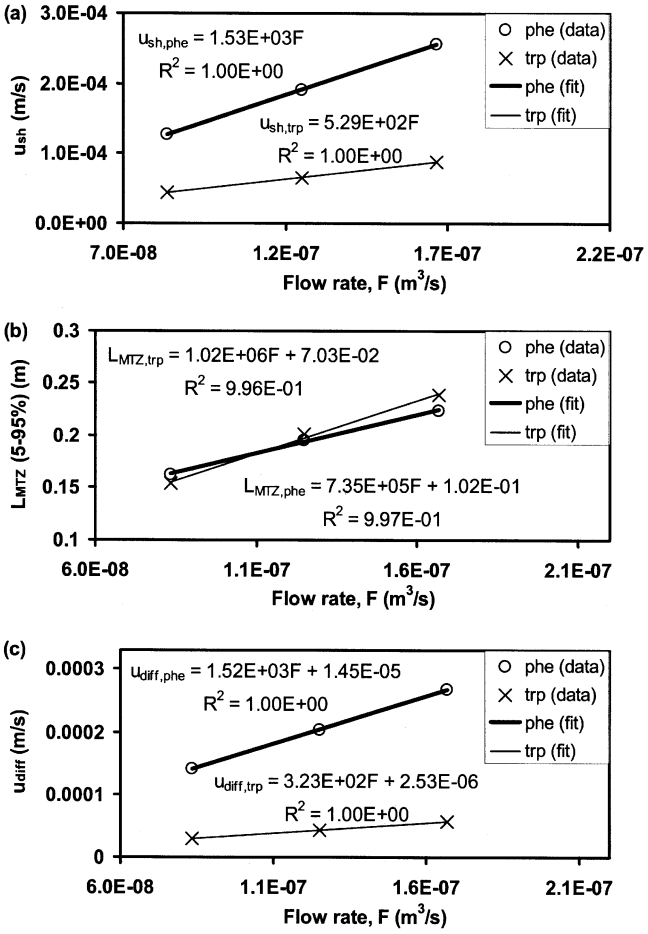

Figure 4. Summary of long pulse experimental results as a function of flow rate.

(a) Shock wave velocity, (b) mass-transfer zone length, and (c) diffuse wave velocity.

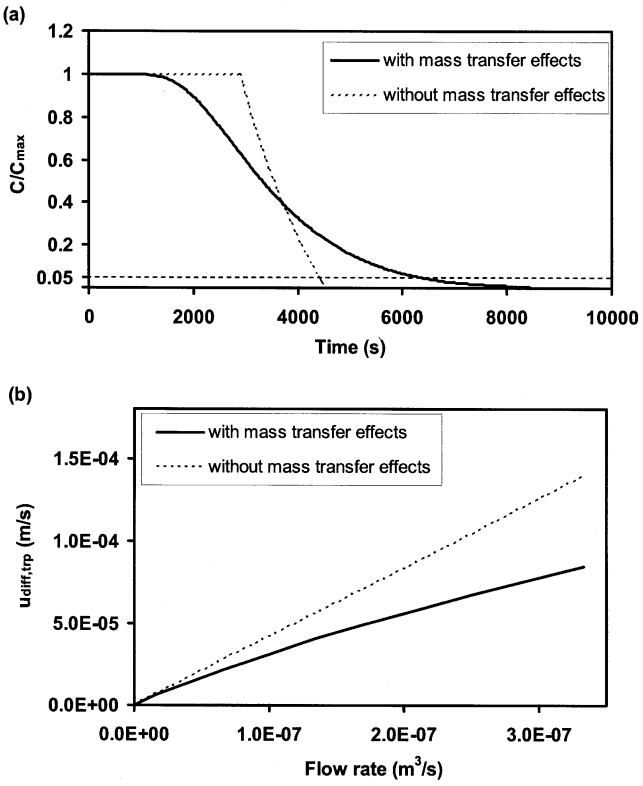

Figure 5. Comparison of diffuse waves with and without mass-transfer effects.

(a) Elution curves of trp at 1.67×10^{-7} m^3/s and (b) diffuse wave velocity for $C/C_{max} = 0.05$ as a function of flow rate.

Table 3. Summary of Operation Conditions for SMB Run 1 and Run 2

		Run 1		Run 2	
		Ideal	Nonideal	Ideal	Nonideal
Inlet and outlet flow rate (10^{-7} m^3/s)	Feed	3.30	3.30	1.33	1.33
	Desorbent	4.84	6.77	1.92	3.79
	Extract	4.94	6.48	1.96	3.72
	Raffinate	3.23	3.58	1.29	1.40
Zone flow rate (10^{-7} m^3/s)	I	6.64	8.58	2.63	4.71
	II	1.70	2.10	0.67	0.99
	III	5.03	5.40	2.00	2.32
	IV	1.81	1.82	0.71	0.92
Switching time (10^3 s)		1.14	1.09	2.88	2.05
Column dimension (i.d. $\times$ L_c m)		0.0268 $\times$ 0.305		0.0268 $\times$ 0.305	
ϵ_b		0.34		0.34	
ϵ_p		0.55		0.55	
Zone configuration		3-2-3-2		2-2-2-2	
Extra column dead volume (10^{-6} m^3/column)		10.0		8.0	

without mass-transfer effects (defined as Curve-WO) is obtained from the equilibrium analysis, whereas the elution curve of trp with mass-transfer effects (defined as Curve-W) is obtained from the rate model simulation.

As shown in Figure 5a, Curve-WO is relatively sharp, whereas Curve-W has a great deal of spreading. As a result, the elution time associated with the 5% plateau concentration (t_{diff}) is shorter for Curve-WO than for Curve-W. Since the diffuse wave velocity (u_{diff}) is defined as the quotient of the column length (L_c) over t_{diff}, the value estimated from Curve-WO is higher than that estimated from Curve-W. The u_{diff} is plotted against a wide range of flow rates (Figure 5b). As the flow rate approaches zero, the difference between the u_{diff} estimated from Curve-WO and that from Curve-W diminishes. The function of u_{diff} vs. flow rate is nonlinear in the entire flow rate range for a nonideal system. However, the curve of u_{diff} vs. flow rate can be linearized locally in practice. In the long pulse tests of this study, the flow rate ranges from 8.33×10^{-8} m^3/s to 1.67×10^{-7} m^3/s. If the straight line fitted from the data within this range is extrapolated to the point of zero flow rate, a non-zero u_{diff} is obtained.

SMB experiment based on the shortcut design

The empirical correlations obtained from the long pulse experiments were used to calculate the zone flow rates and switching time from Eqs. 15a–15e. The calculated values are listed in Table 3 (Run 1).

SMB experiment Run 1 was carried out on SMB1. The high affinity product trp was collected in the extract and the low affinity product phe was collected in the raffinate. The effluent histories at the extract and raffinate ports, and the mid-step column profiles at the cyclic steady state (the 30th step) are shown in Figure 6. The concentrations in the effluent histories are averaged over one switching time, while those in the column profiles are the instantaneous concentrations. Rate model simulations were conducted in parallel. In this model, the actual port switching in an SMB process is simulated (Hritzko et al., 2002; Xie et al., 2002). The model predictions (lines in Figure 6) are in close agreement with the experimental data (symbols in Figure 6) of both the effluent histories and the column profiles at mid-step. Along with Figure 3, Figure 6 indicates that the detailed rate model and the model parameters listed in Table 1 are valid.

The experimental results are summarized in Table 4. The purities of the raffinate and extract were 99.1% and 100%, respectively. The yields of phe and trp were 100% and 96.3%, respectively. The trp yield depends on how the diffuse wave velocity of trp is estimated and what concentration point of trp along its elution wave in the long pulse experiments is targeted. In this study, the targeted concentration point of the trp elution wave is 5% of the trp feed concentration, which means that 5% of the trp feed could be lost in the raffinate

Table 4. Summary of the Simulation and Experimental Results*

		Run 1		Run 2	
		Ideal	Nonideal	Ideal	Nonideal
Feed concentration (kg/m^3)	phe	(5.50)	5.50 (5.50)	(4.98)	4.98 (4.98)
	trp	(2.06)	2.06 (2.06)	(1.98)	1.98 (1.98)
Product concentration (kg/m^3)	phe	(5.60)	5.07 (4.99)	(5.13)	4.75 (4.79)
	trp	(1.31)	1.01 (0.95)	(1.32)	0.72 (0.72)
Purity (%)	phe	(97.9)	99.1 (98.0)	(98.8)	99.5 (99.9)
	trp	(95.0)	100 (99.3)	(98.3)	99.1 (99.5)
Yield (%)	phe	(98.2)	100 (99.8)	(99.4)	98.8 (99.6)
	trp	(94.3)	96.3 (94.1)	(96.8)	99.6 (99.6)

*Values in parentheses are from simulations.

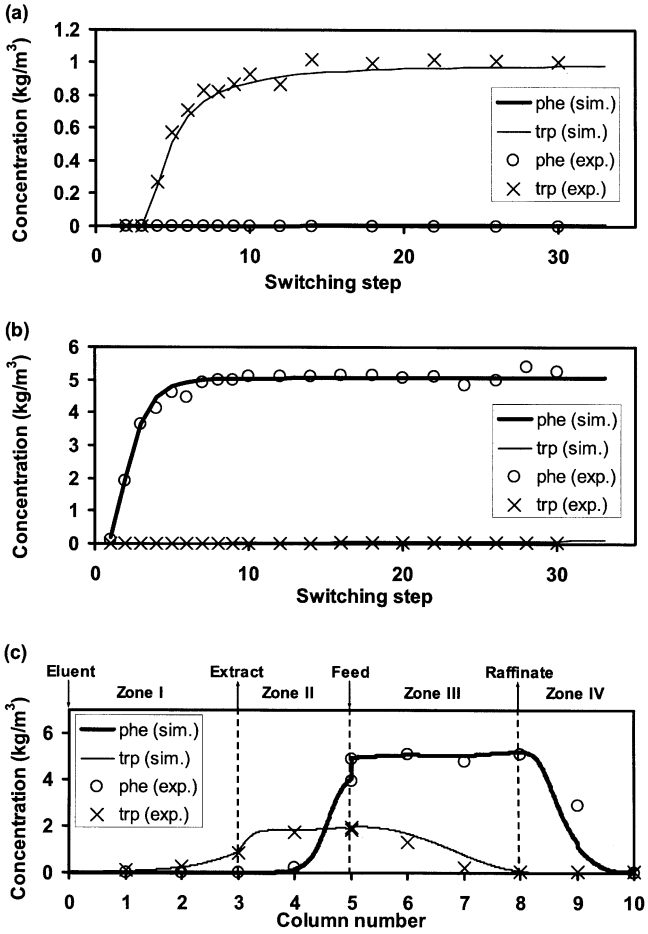

Figure 6. Experimental data and simulation results of SMB Run 1.

(a) Effluent history of the extract, (b) effluent history of the raffinate, and (c) the 30th mid-step column profiles. exp.—experiment, sim.—simulation.

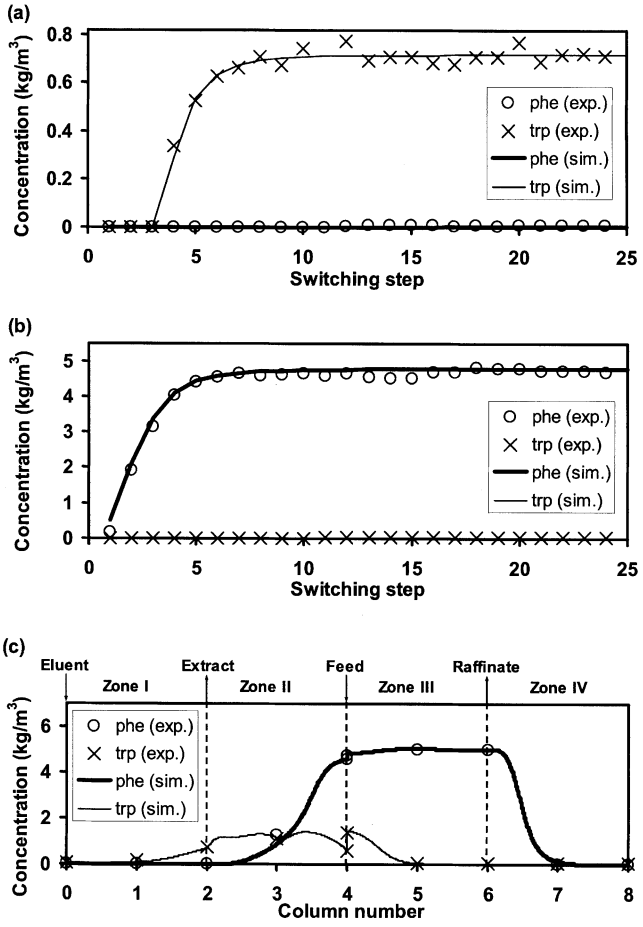

Figure 7. Experimental data and simulation results of SMB Run 2.

(a) Effluent history of the extract, (b) effluent history of the raffinate, and (c) the 24th mid-step column profiles. exp.—experiment, sim.—simulation.

of the SMB. The trp yield can be improved by targeting a lower concentration point of trp along its elution wave. In this case, the flow rates of eluent and zone I should be increased. The SMB experimental results, showing high purity and high yield, prove that the experimental shortcut design method is feasible, efficient, and practical for nonideal systems. It does not require the knowledge of either the isotherm parameters or the mass-transfer parameters. Only three or more long pulse experiments at different flow rates are needed.

Note that this method is limited to a constant feed composition. If the feed composition changes over a wide range, a series of long pulse experiments with different feed compositions will be needed.

Validation of the SWD with SMB experiment

An SMB experiment for the separation of phe and trp was carried out to validate the SWD for nonideal systems. The operating conditions are determined from the SWD and are listed as Run 2 in Table 3. SMB2 was used in this experiment.

This SMB experiment lasted 24 switching steps or 3 full cycles and reached cyclic steady state. The effluent histories of the extract and the raffinate are shown in Figures 7a and 7b. The extract purity and yield were 99.1% and 99.6%, respectively; while the raffinate purity and yield were 99.5% and 98.8%, respectively. Column profile samples were collected at the mid-step of the 24th switching. Figure 7c shows the concentration data from the samples. The simulation results are also plotted in Figure 7. Both the effluent histories and the column profiles are in close agreement with the experimental data, which indicates that the design method and the model parameters are valid.

Comparison of the shortcut design and the SWD in the triangular region

The operating conditions of Run 1 and Run 2 are plotted in the triangular region determined by the triangle theory (Figure 8). As shown in Figure 8, the operating conditions of Run 1 obtained from the shortcut design are on the boundary of the triangular region and close to the pure extract region. According to the experimental shortcut design procedure as

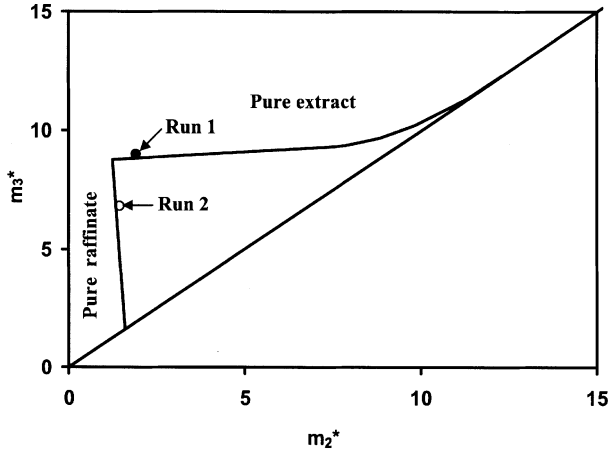

Figure 8. Operating conditions of the SMB experiments Run 1 and Run 2 in the triangular region of the triangle theory.

described in the theory section, the zone II flow rate is determined by the difference between the zone III flow rate and the feed flow rate. The value of the zone II flow rate (2.10×10^{-7} m^3/s) determined in this way is larger than the minimum value (1.75×10^{-7} m^3/s) specified by Eq. 16. The resulting diffuse wave velocity of phe in zone II is higher than the average port moving velocity; thus, the operating conditions of Run 1 are close to the pure extract region in the triangular region.

In contrast, the operating conditions of Run 2 obtained from the standing wave design are within the triangular region, but close to the pure raffinate region. This is consistent with the results shown in the theory section. The linear approximations of the mass-transfer corrections in zones III and IV are higher than what are needed; thus, provide a conservative design.

Further validation of the SWD with simulations and comparison with the triangle theory

Nine cases are investigated at different feed concentrations, particle sizes, and column lengths. The design conditions of the nine cases are listed in Table 5. The ideal design (Eqs. 1–3) and the nonideal design (Eqs. 2, 3, and 5) give two different sets of zone flow rates and switching time. The maximum feed flow rate determined by Eq. 8 is used.

The standing wave solutions of the nine cases are plotted in Figure 9 along with the triangular region specified by the triangle theory. The standing wave equations for the ideal systems (Eqs. 1–3) provide unique solutions. These solutions (solid symbols in Figure 9) are consistent with the vertex points of the triangular regions for the ideal systems. The vertex points correspond to the operating conditions that provide the maximum throughput and the minimum solvent consumption for ideal systems. For nonideal systems, standing wave solutions (open symbols) are within the triangular regions and provide robust operating conditions.

The operating conditions determined by the SWD (for both ideal and nonideal systems) in the above nine cases are applied in the rate model simulations. The results listed in Table 6 show that if the operating conditions determined by the nonideal design are used, the purities and yields of both phe and trp are close to or higher than the target value (99%) for all nine cases. However, if the operating conditions determined by the ideal design are used in the simulations, the purities are lower than those associated with the nonideal design and the values vary widely. The purities resulting from the ideal design can be correlated to the aforementioned dimensionless number (DI).

Dimensionless number analysis

The DI values of the nine cases listed in Table 5 are calculated and shown in Table 6. To further investigate the correlation between DI and the product purities resulting from the ideal design, the product purities and the associated DI values are plotted in Figure 10. The phe desorption wave in zone II affects the extract purity and the trp adsorption wave in zone III affects the raffinate purity. For these reasons, the dimensionless numbers for zone II and zone III are plotted against the extract purity and the raffinate purity, respectively. As DI increases, the deviation from the ideal system increases and the product purity from the ideal design decreases. Note that the maximum feed flow rate is determined by the nonideal design and is applied in the ideal design in

Table 5. Design Conditions with Different Feed Concentrations, Column Lengths, and Particle Sizes

Column Inner Dia. (m)		ϵ_b	ϵ_p	Zone Configuration	Extra Column Dead Volume (m^3/column)
0.0268		0.34	0.55	2-2-2-2	8.0×10^{-6}
Case	R_p (10^{-4} m)	L_c (m)	F_F * (10^{-7} m^3/s)	$C_{\text{feed,phe}}$ (kg/m^3)	$C_{\text{feed,trp}}$ (kg/m^3)
1	1.8	0.305	1.40	7.5	3.0
2	1.8	0.305	1.17	15.0	6.0
3	1.8	0.305	0.85	30.0	12.0
4	0.5	0.305	19.92	5.0	2.0
5	1.5	0.305	2.15	5.0	2.0
6	3.0	0.305	0.52	5.0	2.0
7	1.8	0.05	0.16	5.0	2.0
8	1.8	0.10	0.42	5.0	2.0
9	1.8	0.40	1.98	5.0	2.0

*The maximum feed flow rate (F_F) determined by the SWD for nonideal systems is chosen in each case.

Table 6. Dimensionless Numbers and Simulation Results of Cases in Table 5 with Maximum Feed Flow Rate

							Purity and Yield from Simulation (%)							
							Ideal Design				Nonideal Design			
	St (10^{-2})		Pe (10^{3})		DI (10^{-2})		Raffinate		Extract		Raffinate		Extract	
Case	Zone II	Zone III	Zone II	Zone III	Zone II	Zone III	Purity	Yield	Purity	Yield	Purity	Yield	Purity	Yield
1	1.16	0.42	1.01	1.02	0.72	2.95	98.9	99.3	98.0	97.0	99.8	99.9	99.6	99.3
2	1.06	0.45	1.01	1.02	0.74	2.58	99.1	99.3	98.1	97.7	99.8	99.7	99.3	99.4
3	0.97	0.51	1.01	1.02	0.76	2.07	99.1	99.3	98.0	97.8	99.8	99.7	99.3	99.6
4	0.33	0.11	3.68	3.74	0.64	3.06	98.4	99.3	98.1	96.0	99.8	99.9	99.8	99.3
5	1.01	0.34	1.21	1.23	0.69	3.07	98.4	99.2	98.0	96.0	99.8	99.9	99.8	99.4
6	2.04	0.70	0.60	0.61	0.77	3.11	98.4	99.2	97.7	95.9	99.8	99.9	99.8	99.3
7	8.64	3.36	0.16	0.16	1.21	2.87	99.0	97.1	92.2	96.9	99.9	99.8	99.3	99.5
8	3.89	1.40	0.33	0.33	0.92	2.99	98.7	98.6	96.1	96.5	99.8	99.9	99.8	99.4
9	0.92	0.31	1.33	1.34	0.68	3.09	98.4	99.3	98.1	95.9	99.8	99.9	99.8	99.4

each case. The maximum feed flow rate decreases as the system nonideality increases. The resulting *DI* values are thus limited within a narrow range as shown by the open triangles in Figure 10.

Since the maximum feed flow rate cannot be pre-determined from the ideal design, the operating conditions of the nine cases are recalculated using the ideal design for a fixed feed flow rate. The *DI* values based on these operating conditions are calculated and listed in Table 7. The product purities are plotted against the *DI* values in Figure 10 (solid diamonds). Without the constraint of the maximum feed flow rate, the *DI* values are widely distributed. The product purity decreases as the *DI* value increases. As the *DI* value approaches zero, the product purity is close to 100%. On the other hand, if the *DI* value is greater than 0.005, the product purity drops below 99%. Therefore, if the *DI* calculated from the ideal design has a value greater than 0.005, the system significantly deviates from the corresponding ideal system and the nonideal design should be used to achieve high product purities for both the raffinate and the extract. Note that the critical *DI* value (0.005) is estimated only for phe-trp system, and it might be different for other systems.

The ideal design was performed to recalculate the operating conditions with the same feed flow rates as those in Run 1 and Run 2. These operating conditions are listed in Table 3. In the Run 1 ideal design, the *DI* values of zones II and III are 0.015 and 0.068, respectively. These values are much larger than 0.005; accordingly, low purities are expected from Figure 10. The rate model simulation was carried out with the operating conditions determined from the ideal design. The simulated purities of phe and trp are 97.9% and 95.0%, respectively (Table 4).

In the Run 2 ideal design, the *DI* values of zones II and III are 0.006 and 0.028, respectively. Since the feed flow rate in Run 2 is much lower than that in Run 1, but the same column and particle size are used in both runs, the *DI* values of the ideal Run 2 are much lower than those of the ideal Run 1. As a result, the simulated product purities of the ideal Run 2 are higher than those of the ideal Run 1 (Table 4). However, the *DI* values of the ideal Run 2 are still greater than 0.005. This indicates that the system deviates from the corresponding ideal system; thus, the product purities based on the nonideal design are still higher than those from the ideal design, as shown in Table 4.

Conclusions

If the isotherm and mass-transfer parameters are unknown, an experimental shortcut design method can be used to determine the SMB operating conditions for nonideal systems. Three or more long pulses of a binary mixture at different flow rates are needed to obtain a set of empirical correlations, which are then used to calculate zone flow rates and switching time. An SMB experiment for the binary separa-

Table 7. Dimensionless Numbers and Simulation Results of Cases in Table 5 with Fixed Feed Flow Rate*

							Purity and Yield from Simulations Based on Ideal Design (%)			
	St (10^{-2})		Pe (10^{3})		DI (10^{-2})		Raffinate		Extract	
Case	Zone II	Zone III	Zone II	Zone III	Zone II	Zone III	Purity	Yield	Purity	Yield
1′	1.16	0.42	1.01	1.02	0.72	2.95	98.8	99.3	98.0	97.0
2′	0.89	0.38	1.01	1.02	0.86	3.06	98.9	99.1	97.5	97.1
3′	0.60	0.31	1.02	1.02	1.17	3.32	98.4	98.5	95.9	95.9
4′	4.48	1.54	3.61	3.63	0.07	0.25	99.9	100	99.9	99.8
5′	1.54	0.52	1.21	1.22	0.48	2.04	99.2	99.5	98.7	98.0
6′	0.78	0.26	0.61	0.61	1.74	7.92	94.7	97.8	93.9	86.3
7′	1.07	0.41	0.17	0.17	5.48	19.22	89.9	93.5	80.7	72.7
8′	1.19	0.42	0.33	0.33	2.32	9.17	94.3	96.9	91.2	84.8
9′	1.30	0.44	1.32	1.34	0.50	2.21	99.1	99.5	98.7	97.7

*Feed flow rate is fixed at 1.40×10^{-7} m^3/s.

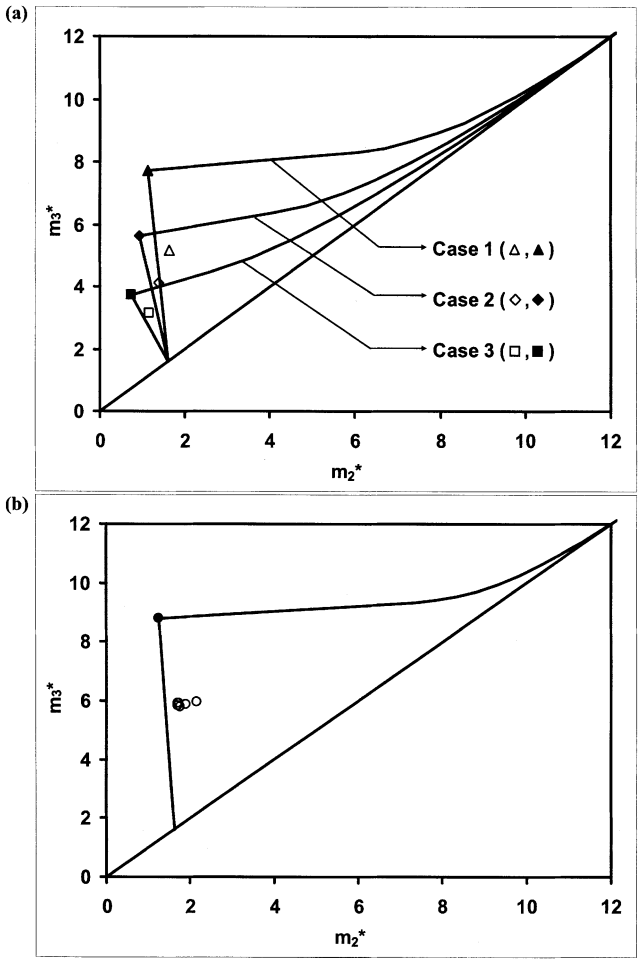

Figure 9. Standing wave design results in the triangular region of the triangle theory for (a) Cases 1–3 in Table 5 and (b) Cases 4–9 in Table 5.

The solid symbols are obtained from the SWD for the ideal system and the open symbols from the SWD for the nonideal system.

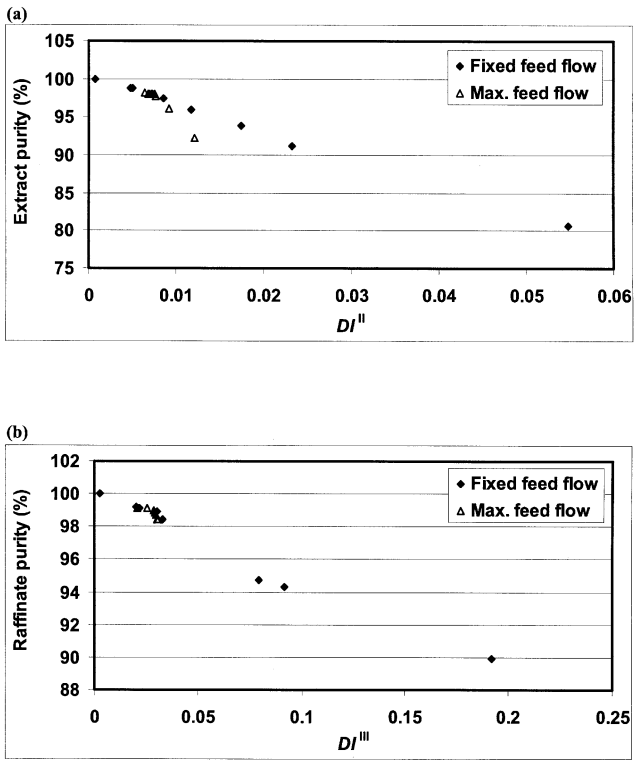

Figure 10. Product purities resulting from the ideal design as a function of the dimensionless number *DI*.

(a) Extract purity and (b) raffinate purity.

tion of phe and try was carried out to validate this design method. High purity (99.1%–100%) and high yield (96.3%–99.6%) were achieved for phe and trp. This shortcut design method is simple and efficient. However, it is limited to the separation of a mixture with a fixed feed concentration.

A standing wave design method is developed for nonlinear, nonideal systems, of which the isotherm and mass-transfer parameters are known. This method is more efficient and less computationally intensive than other literature methods. It also gives unique robust operating conditions rather than a range of possible conditions. Rate model simulations show that the standing wave design can achieve its targeted purity and yield, and always gives higher purity and higher yield than a design ignoring mass-transfer effects. An SMB experiment based on the standing wave design was conducted for the phe-trp separation. High purity (99.1%–99.5%) and high yield (98.8%–99.6%) were achieved.

The standing wave design method developed in this study is a generic design method that can be used to determine the zone flow rates and switching times for given SMB units. In future work, optimization schemes, which include cost functions for adsorbent, desorbent, and equipment, can be developed based on the standing wave design to search for optimal column length, particle size, zone configuration, and so on.

A dimensionless number is derived from the standing wave design equations. The value of the dimensionless number indicates the deviation of an actual system from its corresponding ideal system and the necessity of considering mass-transfer effects in the design. If the dimensionless number in either zone II or zone III is greater than 0.005 for the phe-trp system, the nonideal design can give significantly higher product purity and yield than the ideal design.

Acknowledgment

This project was supported in part by the grants from NSF 0215146 and Indiana 21st Century Research and Technology Fund.

Notation

a_i = Langmuir isotherm parameter of component i, m^3/m^3 S.V.
b_i = Langmuir isotherm parameter of component i, m^3/kg
$C_{p,i}$ = plateau concentration of component i as defined in Figure 1, kg/m^3
$C_{s,i}$ = plateau concentration of component i as defined in Figure 1, kg/m^3

$D_{p,i}$ = intraparticle diffusivity of component i, m^2/s
$D_{\infty,i}$ = Brownian diffusivity of component i, m^2/s
DI_i^j = dimensionless number defined in Eq. 10
DV = extra column dead volume, m^3
$E_{b,i}^j$ = axial dispersion coefficient of component i in zone j, m^2/s
F_F = feed flow rate, m^3/s
F_R = raffinate flow rate, m^3/s
F^j = flow rate in zone j, m^3/s
$k_{f,i}^j$ = film mass-transfer coefficient of component i in zone j, m/s
k_i^j = lumped mass-transfer coefficient of component i in zone j, s^{-1}
L_c = length of an individual column, m
L^j = length of zone j, m
$L_{\mathrm{MTZ},i}$ = mass-transfer zone length of component i, m
$P \equiv (1-\epsilon_b)/\epsilon_b$ = particle/mobile-fluid volume ratio
Pe_i^j = the Peclet number for component i in zone j
R_p = particle radius, m
S = column cross-sectional area, m^2
St_i^j = the Stanton number for component i in zone j
u_0^j = liquid interstitial velocity in zone j, m/s
$u_{\mathrm{diff},i}$ = diffuse wave velocity of component i, m/s
$u_{sh,i}$ = shockwave velocity of component i, m/s
x = coefficient in Eqs. 12–14
y = coefficient in Eqs. 13–14
Y_i = yield of component i
β_i^j = decay factor of standing wave i in zone j
δ_i^j = defined in Eq. 2 for component i in zone j
ϵ_b = interparticle void fraction
ϵ_p = intraparticle void fraction
ν = average port movement velocity, m/s

Literature Cited

Azevedo, D. C. S., and A. E. Rodrigues, "Design of a Simulated Moving Bed in the Presence of Mass-Transfer Resistances," *AIChE J.*, **45**, 956 (1999).

Azevedo, D. C. S., and A. E. Rodrigues, "Fructose-Glucose Separation in a SMB Pilot Unit: Modeling, Simulation, Design, and Operation," *AIChE J.*, **47**, 2042 (2001).

Biressi, G., O. Ludemann-Hombourger, M. Mazzotti, R.-M. Nicoud, and M. Morbidelli, "Design and Optimisation of a Simulated Moving Bed Unit: Role of Deviations from Equilibrium Theory," *J. Chromatogr. A.*, **876**, 3 (2000).

Broughton, D. B., and C. G. Gerhold, "Continuous Sorption Process Employing Fixed Bed of Sorbent and Moving Inlets and Outlets," U.S. Patent No. 2,985,589 (1961).

Chin, C., "Versatile Simulated Moving Bed Systems," MS Thesis, Purdue University, West Lafayette, IN (2001).

Ching, C. B., D. M. Ruthven, and K. Hidajat, "Experimental Study of a Simulated Counter-Current Adsorption System—III. Sorbex Operation," *Chem. Eng. Sci.*, **40**, 1411 (1985).

Chung, S. F., and C. Y. Wen, "Longitudinal Dispersion of Liquid Flowing through Fixed and Fluidized Beds," *AIChE J.*, **14**, 857 (1968).

Ganetsos, G., and P. E. Barker, *Preparative and Production Scale Chromatography*, Marcel Dekker, New York (1993).

Hritzko, B., D. Walker, and N.-H. L. Wang, "Design of a Carousel Process for Cesium Removal Using Crystalline Silicotitanate," *AIChE J.*, **46**, 552 (2000).

Hritzko, B., Y. Xie, R. Wooley, and N.-H. L. Wang, "Standing Wave Design of Tandem SMB for Linear Multicomponent Systems," *AIChE J.*, **48**, 12 (2002).

Imamoglu, S., "Simulated Moving Bed Chromatography (SMB) for Application in Bioseparation," *Advances in Biochem. Eng. Biotech.*, Vol. 76, T. Scheper and R. Freitag, eds., Springer, New York (2002).

Juza, M., M. Mazzotti, and M. Morbidelli, "Simulated Moving Bed Chromatography and Its Application to Chirotechnology," *Trends Biotechnol.*, **18**, 108 (2000).

Ma, Z., and N.-H. L. Wang, "Standing Wave Analysis of SMB Chromatography: Linear Systems," *AIChE J.*, **43**, 2488 (1997).

Mallmann, T., B. D. Burris, Z. Ma, and N.-H. L. Wang, "Standing Wave Design of Nonlinear SMB Systems for Fructose Purification," *AIChE J.*, **44**, 2628 (1998).

Mazzotti, M., G. Storti, and M. Morbidelli. "Optimal Operation of Simulated Moving Bed Units for Nonlinear Chromatographic Separations," *J. Chromatogr. A*, **769**, 3 (1997).

Migliorini, C., A. Gentilini, M. Mazzotti, and M. Morbidelli, "Design of Simulated Moving Bed Units under Non-Ideal Conditions," *Ind. Eng. Chem. Res.*, **38**, 2400 (1999).

Migliorini, C., M. Mazzotti, G. Zenoni, and M. Morbidelli, "Shortcut Experimental Method for Designing Chiral SMB Separations," *AIChE J.*, **48**, 69 (2002).

Nicoud, R. M., "Simulated Moving Bed (SMB): Some Possible Applications for Biotechnology," *Bioseparation and Bioprocessing*, G. Subramanian, ed., Wiley-VCH, New York (1998).

Pais, L. S., J. M. Loureiro, and A. E. Rodrigues, "Separation of 1,1′-bi-2-naphthol Enantiomers by Continuous Chromatography in Simulated Moving Bed," *Chem. Eng. Sci.*, **52**, 245 (1997).

Pynnonen, B., "Simulated Moving Bed Processing: Escape from the High-Cost Box," *J. Chromatogr. A*, **827**, 143 (1998).

Rhee, H. K., R. Aris, and N. Amundson, "Multicomponent Adsorption in Continuous Countercurrent Exchangers," *Phil. Trans. Roy. Soc. London. A*, **269**, 187 (1971).

Ruthven, D. M., and C. B. Ching, "Countercurrent and Simulated Countercurrent Adsorption Separation Processes," *Chem. Eng. Sci.*, **44**, 1011 (1989).

Schulte, M., J. N. Kinkel, R.-M. Nicoud, and F. Charton, "Simulated Moving-Bed Chromatography: An Efficient Technique for Producing Optically Active Compounds on an Industrial Scale," *Chem. Ind. Tech.*, **68**, 670 (1996).

Schulte, M., and J. Strube, "Preparative Enantioseparation by Simulated Moving Bed Chromatography," *J. Chromatogr. A*, **906**, 399 (2001).

Storti, G., M. Mazzotti, S. Carra, and M. Morbidelli, "Optimal Design of Multicomponent Counter-Current Adsorption Separation Processes Involving Nonlinear Equilibria," *Chem. Eng. Sci.*, **44**, 1329 (1989).

Storti, G., M. Mazzotti, M. Morbidelli, and S. Carrà, "Robust Design of Binary Countercurrent Adsorption Separation Processes," *AIChE J.*, **39**, 471 (1993).

Wilson, E. J., and C. J. Geankoplis, "Liquid Mass Transfer at Very Low Reynolds Numbers in Packed Beds," *Ind. Eng. Chem. Fundam.*, **5**, 9 (1996).

Wu, D.-J., Y. Xie, Z. Ma, and N.-H. L. Wang, "Design of Simulated Moving Bed Chromatography for Amino Acid Separations," *Ind. Eng. Chem. Res.*, **37**, 4023 (1998).

Xie, Y., D.-J. Wu, Z. Ma, and N.-H. L. Wang, "Extended Standing Wave Design Method for Simulated Moving Bed Chromatography: Linear Systems," *Ind. Eng. Chem. Res.*, **39**, 1993 (2000).

Xie, Y., S.-Y. Mun, J.-H. Kim, and N.-H. L. Wang, "Standing Wave Design and Experimental Validation of a Tandem Simulated Moving Bed Process for Insulin Purification," *Biotech. Prog.*, **18**, 1332 (2002).

Yun, T., Z. Bensetiti, G. Zhong, and G. Guiochon, "Effect of Column Efficiency on the Internal Concentration Profiles and the Performance of a Simulated Moving-Bed Unit in the Case of a Linear Isotherm," *J. Chromatogr.*, **758**, 175 (1997).

Zhong, G., and G. Guiochon, "Simulated Moving Bed Chromatography. Effects of Axial Dispersion and Mass Transfer under Linear Conditions," *Chem. Eng. Sci.*, **52**, 3117 (1997).

Manuscript received Nov. 27, 2002, and revision received May 20, 2003.